IEEE Access
Multidisciplinary | Rapid Review | Open Access Journal

Received February 24, 2022, accepted March 9, 2022, date of publication March 24, 2022, date of current version April 1, 2022.

Digital Object Identifier 10.1109/ACCESS.2022.3161966

Nonlinear Model of Vibrating Flip-Flow Screens That Considers the Effects of Screen Panels

DONGDONG LIN[1], NINGNING XU[1], CHI YU[1], RUNHUI GENG[1], XINWEN WANG[1], AND SANPENG GONG[2]

[1]School of Chemical and Environmental Engineering, China University of Mining and Technology, Beijing, Beijing 100083, China
[2]School of Mechanical and Power Engineering, Henan Polytechnic University, Jiaozuo 454003, China

Corresponding author: Xinwen Wang (xinwen.w@cumtb.edu.cn)

This work was supported in part by the Anhui Province Major Science and Technology Achievements Engineering Research and Development Special Project under Grant 202103c08020007, and in part by the Key Scientific and Technological Project of Henan Province under Grant 212102210006.

ABSTRACT Vibrating flip-flow screens have been widely used in the mineral processing industry. As the key components, flip-flow screen panels strongly affect the dynamics of vibrating flip-flow screens. However, there is no systematic research into this problem. In this study, the dynamic characteristics of flip-flow screen panel are identified by the finite element analysis. Furthermore, a nonlinear coupling dynamic model of vibrating flip-flow screens that considers the effects of flip-flow screen panels is proposed, and the analytical and numerical solutions of its governing equation are deduced via the equivalent linearization method and the time marching method. Also, experimental results show that the proposed model describes the movements of vibrating flip-flow screens more accurately than the classical mechanical model which does not consider flip-flow screen panels. Finally, the effects of the screen panel's parameters, such as the slack length and the stiffness, on the dynamics of vibrating flip-flow screens are investigated.

INDEX TERMS Dynamics, finite element analysis, kinematics, mathematical model, nonlinear equations, numerical simulation, piecewise linear approximation, springs, time series analysis, vibrations.

I. INTRODUCTION

Dry separation techniques have been used in various mineral beneficiation processes, and screening based on the particle shape and size plays an important role in the large-scale separation of minerals [1]–[5]. However, conventional screening equipment (linear vibrating or circular vibrating screens) frequently encounters the problem of rapid blockage of screen apertures, which reduces the screening efficiency and increases the labor intensity of workers [6]–[8]. The main and floating screen frames of vibrating flip-flow screens (VFFSs) generate relative movement along the screen surface under the exciter's simple harmonic excitation [9]–[11]. This relative movement causes flip-flow screen panels (FFSPs), which are mounted on the beams of main and floating screen frames, to perform periodic slack and stretch motions. The reciprocating movement of FFSP enables the screen panels to achieve high projection strengths, promoting the loosening and layering of cohesive and wet fine-grained materials, and increasing the penetrating probability of fine-grained materials [12], [13]. Also, the screen panel is cyclically deformed with a large deflection, causing the screen apertures to undergo tensile deformation, which effectively prevents adhesive materials with a large specific surface area and near-aperture particles from blocking the apertures and improves the screening efficiency and throughput [14], [15]. Therefore, VFFS is a common unit operation for dry screening of high-viscosity, high-water, and fine minerals [16], [17].

To date, many researchers have used linear and nonlinear vibration theories to investigate the dynamics of flip-flow screens [18], [19]. Considering the frequency dependence of rubber springs, Tang *et al*. [20] constructed different mathematical models of VFFS under startup and shutdown modes as well as steady working conditions, thereby exploring the influence of rubber spring damping on screen body vibrations. However, these extensive studies only focused on the

The associate editor coordinating the review of this manuscript and approving it for publication was Gerard-Andre Capolino.

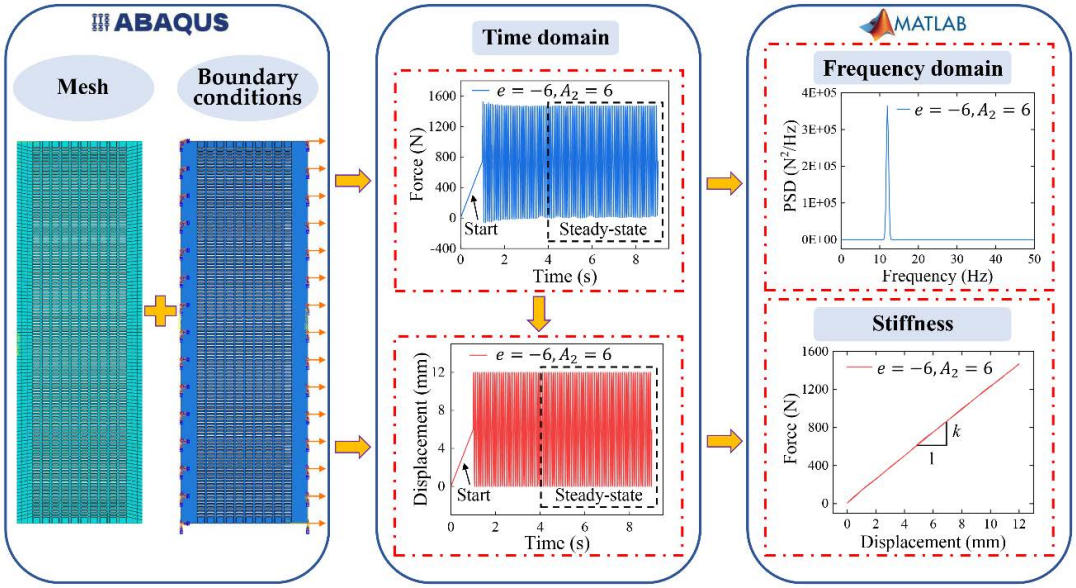

FIGURE 1. Schematic of the finite element simulation of the dynamic characteristics of flip-flow screen panel.

inertial forces of the main and the floating screen frame, the stiffness, and the damping forces of the shear and isolation springs when establishing the mechanical model of VFFS [21]–[24]. Few scholars have drawn any systematic research into the effect of FFSPs on the dynamics of the screen body under working conditions.

FFSPs made of polyurethane material are critical elastic components of VFFS [19], [20]. With the nonlinear material and the large deflection in the screening process, we found the nonlinear flexural and tensile stress of screen panels strongly affected the dynamic characteristics of VFFS when the relative displacement between the main and floating screen frames was beyond the slack length of the FFSP in the experiment. Also, the results of field experiments showed that the classification effect and the kinematic characteristics of the flip-flow screens were strongly influenced by the FFSP tension [25].

Previously published studies about FFSPs primarily focused on the kinematic characteristics and the optimization of process parameters [26], [27], provided good guidance for the advanced design techniques and methods of flip-flow screens [28], [29]. Considering that FFSP thickness was far smaller than its length [30], the unitization method along the width direction was used to establish the corresponding kinematic model of FFSP, allowing the motion of the screen panel to be obtained. For example, Chen *et al.* [31] investigated the vibration characteristics of the screen panel of the LIWELL flip-flow screen based on the string vibration model and the Hamilton principle. Other methods were based on DEM and FEM to investigate the motion and stresses of FFSP followed by the screening performance when the VFFS was operating [20], [32]. Wu *et al.* [33] proposed an approximate flexible method of discretizing FFSP into several rigid screen bars and developed a joint simulation between the materials and FFSP using multibody dynamics. As critical elastic components of VFFS, the elastic deformation of the screen panels was not considered in all of the aforementioned studies on the dynamics of VFFS.

However, the elastic restoring force generated from the tensile deformation of FFSP will have a nonlinear effect on the screen body's dynamic response when the relative displacement between the main and the floating screen frame is beyond the FFSP slack length. If the maximum relative displacement of FFSP exceeds a certain distance during its precession, it typically causes fatigue damage and affects the continuity of the equipment [20], [25]. Thus, a detailed understanding of the dynamic response of VFFS is required.

To resolve these deficiencies, this study first investigates the mechanical properties of FFSP based on the Mooney-Rivlin constitutive model of hyperelastic materials. A more reasonable nonlinear coupling dynamic model of VFFS that considers the effect of FFSP is also proposed, the accuracy of which is verified by experiments. Also, based on the proposed model, the influence of the dynamic parameters of FFSP on the dynamics of VFFS is explored. The results of this study will help describe the dynamic response and the improvement of reliability design and optimization of flip-flow screens.

II. DYNAMIC ANALYSIS OF FLIP-FLOW SCREEN PANEL

The dynamic characteristics of FFSP are investigated by FEM, the scheme of which is shown in Fig. 1. The figure shows the time series of the displacement at the moving end and the force at the fixed end of FFSP under different boundary conditions. Power spectrum analysis is also used to evaluate the energy distribution of the force signal in the frequency

domain [34]. For this analysis, a Hamming window with a length of $N = 2^{12} = 4096$ samples and an overlap of 50% is chosen, which has a high amplitude accuracy [35], [36]. In addition, the number of discrete Fourier transform points is nfft = 8192, and the original signal sampling frequency is fs = 2000 Hz [37]–[41].

A. NONLINEAR FINITE ELEMENT MODEL OF FLIP-FLOW SCREEN PANEL

The continuum mechanics model based on phenomenological theory holds that polyurethane material is isotropic [30], [42]; thus, the Mooney-Rivlin constitutive model with two parameters is used to fit the material properties of FFSP [20], [43]–[45]:

$$W = C_{10}(I_1 - 3) + C_{01}(I_2 - 3) \tag{1}$$

where W is the strain energy potential of polyurethane; I_1 and I_2 are the first and second strain invariants of polyurethane, respectively; and C_{10} and C_{01} are used to describe the shear properties of polyurethane:

$$C_{10} \approx 4C_{01} \tag{2}$$

Experimental results show that the hardness and Young's modulus of the polyurethane material used for FFSP satisfy the following relationships [46]:

$$E\,(psi) \approx 11.427H_A - 0.445H_A^2 + 0.0071H_A^3 \approx 3G \tag{3}$$

$$G \approx 2(C_{10} + C_{01}) \tag{4}$$

where E, H_A, and G are Young's modulus, Shore hardness, and shear modulus, respectively.

The hardness of FFSP is first obtained experimentally, and then, the parameters of the Mooney-Rivlin constitutive model of FFSP are determined through (2), (3), and (4). The geometric dimensions and material properties of the finite element model of FFSP are shown in Table 1.

TABLE 1. Parameters for the finite element model of flip-flow screen panel.

Parameter	Unit	Value
length	mm	328
width	mm	800
thickness	mm	4
density	kg·m^{-3}	1200
screen aperture	mm^2	3×20
shore hardness	/	89
Young's modulus	MPa	17.22
C_{10}	MPa	2.3
C_{01}	MPa	0.57

B. BOUNDARY CONDITIONS OF FLIP-FLOW SCREEN PANEL

The flip-flow principle of FFSP is described in Fig. 2, in which the displacements of the beams of the main screen frame and the floating screen frame along the screen surface

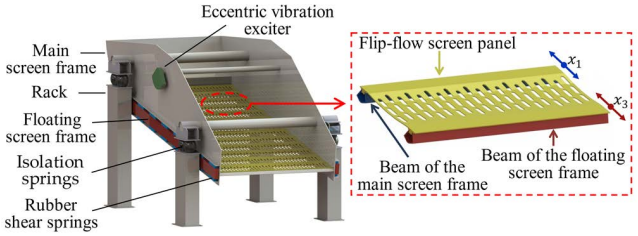

FIGURE 2. Schematic of the flip-flow principle used in vibrating flip-flow screen.

are $x_1 = A_1 sin(\omega t - \alpha_1)$ and $x_3 = A_3 sin(\omega t - \alpha_3)$, respectively. When the relative displacement between these two frames exceeds the FFSP slack length, the force generated from the tensile deformation of FFSP affects the motions of the main and floating screen frames, and then, the movement of FFSP is affected because they are related to one another.

To describe the coupling effects between FFSP and the screen body, the absolute motion at both ends of the screen panel can be transformed into the relative motion, and its motion form can be expressed as:

$$\begin{aligned} x_2 &= x_1 - x_3 = A_1 sin(\omega t - \alpha_1) - A_3 sin(\omega t - \alpha_3) \\ &= A_2 sin(\omega t - \alpha_2) \end{aligned} \tag{5}$$

$$A_2 = \sqrt{(A_1\cos\alpha_1 - A_3\cos\alpha_3)^2 + (A_1\sin\alpha_1 - A_3\sin\alpha_3)^2} \tag{6}$$

$$\alpha_2 = \tan^{-1}\frac{A_1\sin\alpha_1 - A_3\sin\alpha_3}{A_1\cos\alpha_1 - A_3\cos\alpha_3} \tag{7}$$

where A_1 and A_3 are the displacement amplitudes of the main screen frame and the floating screen frame, respectively; α_1 and α_3 are the displacement phases of the main screen frame and the floating screen frame, respectively; A_2 and α_2 are the relative amplitude and the displacement phase difference between the screen frames, respectively; and ω is the angular frequency of the exciter.

Fig. 3 shows the kinematic model of the relative motion of FFSP. The original length of FFSP is L_0, and the FFSP slack length is e. When $e \geq 0$, the screen panel is slackened at the initial moment; otherwise, the screen panel is stretched at the initial moment. The right end of the screen panel oscillates under the sinusoidal excitation of $x_2 = A_2 sin(\omega t - \alpha_2)$, and the other end is fixed. When the displacement of the movable end exceeds the slack length, the FFSP produces tensile deformation, the tensile stress of which will act on the fixed end. The dynamic characteristics of FFSP can be analyzed by sampling the force signal of the left end and the displacement signal of the right end under different boundary conditions [47], [48].

Therefore, the tension value of the screen panel can be written as [25]:

$$\Delta L = A_2(1 + sin\alpha_2) - e \tag{8}$$

Equation (8) shows that the tension value of FFSP is related to the relative amplitude, the displacement phase difference,

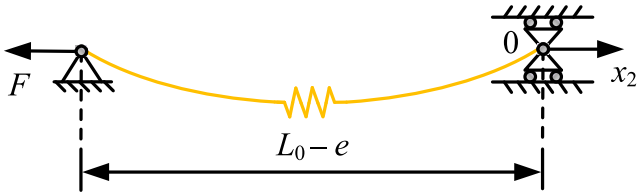

FIGURE 3. Kinematic model of the relative movement of flip-flow screen panel.

and the slack length. This equation can determine whether there is tensile during the movement of the screen panel and provide boundary conditions for the subsequent study of the force of the screen panel When $\Delta L \geq 2A_2$, the screen panel experiences a tensile force throughout its movement, and the force of the screen panel is primarily due to the tensile stress caused by the tensile deformation. When $0 < \Delta L < 2A_2$, there is both tension and slack in the process of the screen panel's movement. The screen panel's force is caused by the flexural stress generated by the inertial force and the tensile stress generated by the tensile deformation of the screen panel. When $\Delta L \leq 0$, the screen panel is always slack during its movement, and the force of the screen panel is only due to the flexural stress generated by the inertial force.

C. DYNAMIC CHARACTERISTICS OF FLIP-FLOW SCREEN PANEL

1) EFFECTS OF THE SLACK LENGTH ON THE DYNAMIC CHARACTERISTICS OF FLIP-FLOW SCREEN PANEL

To identify the effect of the slack length on the dynamic characteristics of FFSP, we consider the real working parameters of VFFS as boundary conditions. In this simulation, the excitation frequency is 12 Hz, the relative amplitude is 6 mm, and the phase angle is 0 rad; thus, the displacement of the moving end is $x_2 = 6sin\,(24\pi t)$. The force acting on the fixed end of FFSP during motion is sampled as the slack lengths are −6, −3, 0, 3, and 6 mm.

The steady-state time series of the force signal of FFSP for different slack lengths are shown in Fig. 4(a). With increasing slack length, the peak value of the force signal gradually decreases, and its fluctuation increases instead. When the slack length is −6 mm, the tension value is 12 mm, the screen panel experiences a tensile stress during its movement, and the signal is periodic. Conversely, when the slack length is 6 mm, the tension value is 0 mm, the screen panel is always slack, and the force can be described as a stable and stochastic signal.

The power spectrum analysis of the force signal of FFSP under different slack conditions is shown in Fig. 4(b). When the slack length is −6 mm, the PSD of the force signal only has a peak at the excitation frequency. However, when the slack lengths are −3, 0, 3, and 6 mm, a frequency domain analysis of the force signal shows that the force consists of a component corresponding to the fundamental frequency (12 Hz) and higher-order harmonic components, which are 24 and 36 Hz, respectively. The peak value

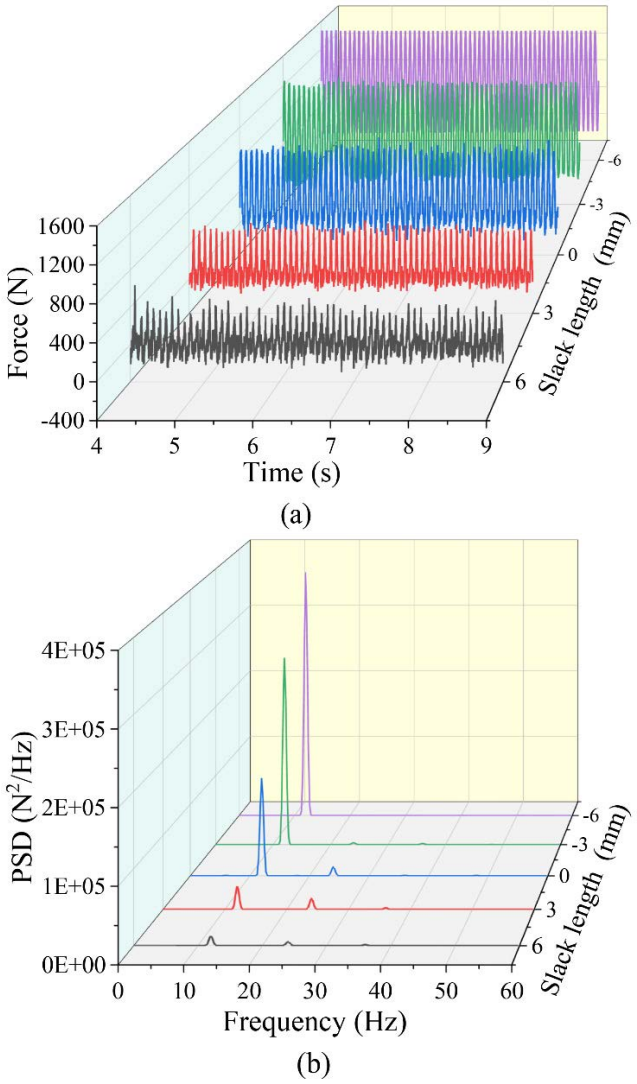

FIGURE 4. Effect of the slack length on the dynamic characteristics of flip-flow screen panel: (a) Time series of the force signal, (b) Power spectral density of the force signal.

corresponding to the fundamental frequency is the largest, followed by the second and third harmonics. When the slack lengths are −6, −3, 0, 3, and 6 mm, the PSDs at the fundamental frequency are 3.65×10^5, 2.71×10^5, 1.37×10^5, 0.31×10^5, and 0.13×10^5 $N^2 \cdot Hz^{-1}$, respectively.

Because the relative amplitude and the excitation frequency of FFSP are constant, the flexural stress gradually changes into tensile stress as the slack length decreases from 6 to −6 mm, whereas the PSD at the fundamental frequency correspondingly increases. When the slack length is 6 mm, the screen panel slackens during its movement, the tension value is 0 mm, and the force is due to the flexural stress, which is caused by the inertial force. Then, when the slack lengths are 3, 0, and −3 mm, the screen panel experiences both tension and relaxation during its movement; its tension values are 3, 6, and 9 mm, respectively; and the PSD at the fundamental frequency is 2.4, 10.5, and 20.8 times that when the slack length is 6 mm, respectively. When the slack length

is −6 mm, the screen panel experiences tension during its movement, and the tension value is 12 mm. The dominant source of the screen panel's force is tensile deformation, and the PSD at the fundamental frequency is 28 times that when the slack length is 6 mm. These results indicate that with constant relative amplitude, angular frequency and displacement phase difference, the tension value of FFSP gradually increases as the slack length changes from positive to negative the tensile stress dominates the force of FFSP, and the flexural stress caused by the inertial force can be ignored.

2) EFFECTS OF THE RELATIVE AMPLITUDE ON THE DYNAMIC CHARACTERISTICS OF FLIP-FLOW SCREEN PANEL

To study the effect of the relative amplitude on the dynamic characteristics of FFSP, the excitation frequency and the phase angle remain unchanged, and the FFSP slack length is 6 mm; thus, the displacement of the moving end is $x_2 = A_2 sin\,(24\pi t)$. The force acting on the fixed end of FFSP during motion is investigated when the relative amplitudes are 4, 6, 8, 10, and 12 mm.

The steady-state time series of the force signal of FFSP under different relative amplitudes are shown in Fig. 5(a). The peak force signal gradually increases with increasing relative amplitude. When the relative amplitude is 4 mm, the FFSP is completely slackened in the movement process, the tension value is −2 mm, and the force fluctuates around zero. As the relative amplitude is 12 mm, there is tension and relaxation during the movement of the screen panel, its tension value is 6 mm, and the peak value is markedly greater than that when the relative amplitude is 4 mm.

Power spectrum analysis of the force signal under different relative amplitudes is performed, the results of which are shown in Fig. 5(b). When the relative amplitude is 4 mm, its tension value is −2 mm, the force is due to the flexural stress caused by inertial force, and its PSD is nearly the horizontal line of zero-crossing. Because the relative amplitudes are 6, 8, 10, and 12 mm, the frequencies corresponding to the peak of PSD are concentrated at 12, 24, and 36 Hz, among which the peak value corresponding to the fundamental frequency is the largest, followed by the second and third harmonics. In contrast to the first two peaks, the peak value matching the third harmonics can be ignored.

When the relative amplitudes are 8, 10 and 12 mm, the tension values are 2, 4 and 6 mm, respectively, and the corresponding PSDs at the fundamental frequency are 0.31×10^5, 0.53×10^5, and 1.79×10^5 $N^2 \cdot Hz^{-1}$, respectively, which are 2.4, 4.1 and 13.8 times that when the slack length is 6 mm. The PSDs at the second harmonics are 0.16×10^5, 0.26×10^5, and 0.39×10^5 $N^2 \cdot Hz^{-1}$.

Because the excitation frequency and slack length are constant, the greater the relative amplitude is, the greater the PSD at the fundamental frequency is. When the relative amplitude is less than the slack length, the tension value of FFSP is less than zero. The force of FFSP is the flexural stress caused by the inertial force, which fluctuates around zero, and its PSD is nearly zero.

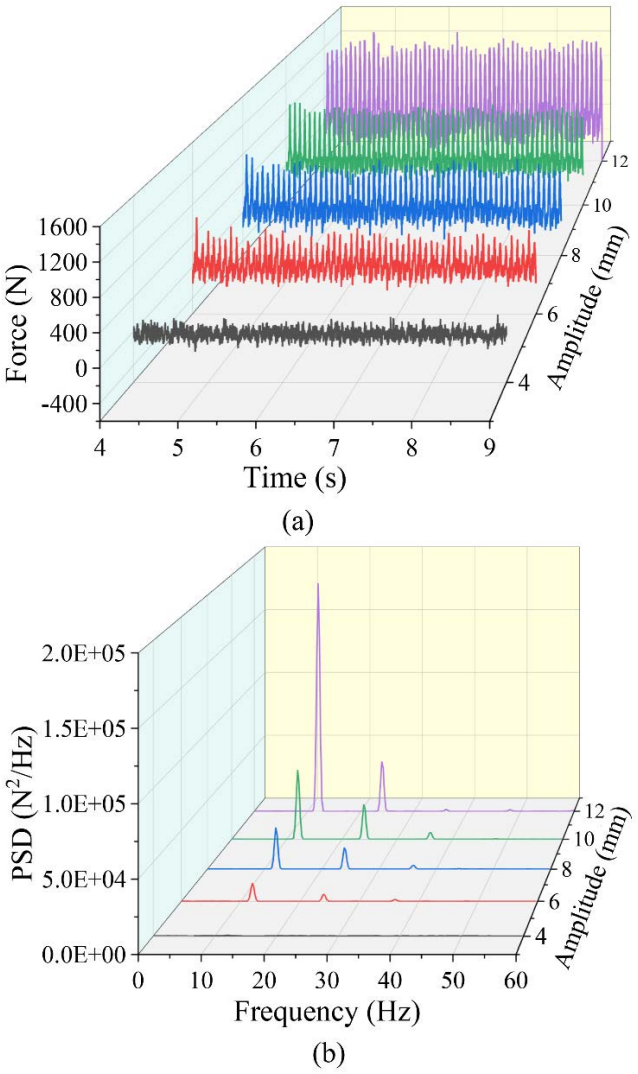

FIGURE 5. Effect of the relative amplitude on the dynamic characteristics of flip-flow screen panel: (a) Time series of the force signal, (b) Power spectral density of the force signal.

3) STIFFNESS OF FLIP-FLOW SCREEN PANEL

To investigate the stiffness of the FFSP, FEM is used to simulate the force of the screen panel. When the excitation frequency is 12 Hz, the slack length is −6 mm, and the relative amplitude is 6 mm. Fig. 6 plots the force as a function of the displacement of the screen panel and shows that the force at the fixed end of the screen panel is directly proportional to the displacement at the moving end, which is approximately a straight line. Therefore, the stiffness of the screen panel is the slope of the straight line, and we can determine that the stiffness of the investigated screen panel is 121,000 $N \cdot m^{-1}$.

Thus, FFSP exhibits strong stiffness under tension, particularly when the slack length is negative. The dynamic characteristics of FFSP thus affect the dynamic response of VFFS; thus, when analyzing the global vibration response of VFFS, the force of the screen panel must be considered.

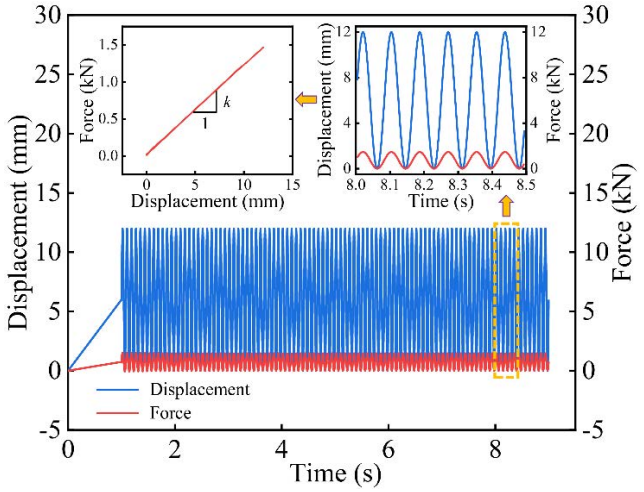

FIGURE 6. Dynamic stiffness of flip-flow screen panel during the tensile state.

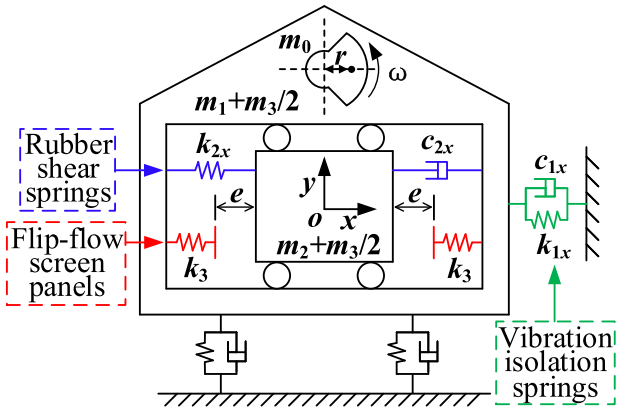

FIGURE 7. Proposed nonlinear dynamic model of vibrating flip-flow screen.

III. DYNAMIC ANALYSIS OF VIBRATING FLIP-FLOW SCREEN

A. NONLINEAR MECHANICAL MODEL OF VIBRATING FLIP-FLOW SCREEN

The investigated vibrating flip-flow screen is shown schematically in Fig. 2. The main screen frame and the floating screen frame are connected by rubber shear springs, and the two ends of FFSP are mounted on the beams of the main screen frame and the floating screen frame, respectively. The vibration isolation springs support the main screen frame on the rack, and the vibration exciter is installed on the main screen frame. The excitation force generated from the eccentric blocks' rotation drives the main and the floating screen frame to produce relative movement and causes the screen panels to perform periodic slack and stretch motions to screen materials.

As mentioned previously, studies of the dynamic characteristics of FFSP have demonstrated that the tensile stress caused by the tensile deformation of the screen panel has a marked impact on the dynamic response of the main and floating screen frames compared with the flexural stress caused by the inertial force. The lumped mass method is used to establish the mechanical model of VFFS considering the tensile effects of flip-flow screen panels [23], [49]. As shown in Fig. 7, the x-axis and y-axis are parallel and perpendicular to the screen surface direction, respectively.

The main screen frame and the floating screen frame are connected through the shear springs. Due to the thin thickness and high stiffness of the shear springs in the y-direction, the main screen frame and the floating screen frame have no relative movement in the y-direction. What's more, the movement of VFFS in the y-direction and the rotation around the center of mass have little effect on the performance of an operating VFFS; therefore, this study only considers the dynamic response of the main screen frame and the floating screen frame in the x-direction [18]. The governing equations of VFFS considering the tensile stress of FFSP can be written as [50]–[52]:

$$\begin{cases} (m_1 + m_2 + m_3)\,\ddot{x}_1 + c_{1x}\dot{x}_1 + k_{1x}x_1 \\ \quad - \left(m_2 + \dfrac{m_3}{2}\right)\ddot{x}_2 = m_0\omega^2 r\sin(\omega t) \\ \left(m_2 + \dfrac{m_3}{2}\right)(\ddot{x}_1 - \ddot{x}_2) - c_{2x}\dot{x}_2 - k_{2x}x_2 \\ \quad - F_k(x_2) = 0 \end{cases} \tag{9}$$

where m_1, m_2, and m_3 are the mass of the main screen frame, the floating screen frame, and the global mass of shear springs and FFSP, respectively; x_1 and x_2 are the displacement of the main screen frame and the relative displacement between the main and the floating screen frame, respectively; $\dot{x}_1$ and $\dot{x}_2$ are the velocity of the main screen frame and the relative velocity between the main and the floating screen frame, respectively; $\ddot{x}_1$ and $\ddot{x}_2$ are the acceleration of the main screen frame and the relative acceleration between these two frames, respectively; k_{1x}, c_{1x}, k_{2x}, and c_{2x} are the stiffness and the damping coefficient of vibration isolation springs and rubber shear springs along the x-direction, respectively; m_0, r, and ω are the mass, the eccentricity, and the angular frequency of the eccentric block, respectively; and $F_k(x_2)$ are the nonlinear elastic restoring force produced by the tensile deformation of FFSP, which can be expressed as:

$$F_k(x_2) = \begin{cases} 0 & |x_2| \le e \\ k_3(x_2 + e) & x_2 < -e \\ k_3(x_2 - e) & x_2 > e \end{cases} \tag{10}$$

where k_3 and e are the stiffness and slack length of the flip-flow screen panels, respectively. When the stiffness of FFSP equals zero, there is no elastic restoring force generated from the tensile deformation of FFSP during the movement of VFFS, and the proposed model turns into the classical model without considering the effect of FFSP.

The vibration differential Equation (9) contains a piecewise linear function of the solution variable (x_2) [53]–[55]. Thus, the analytical solution of nonlinear differential equations is first obtained by the equivalent linear method, and then, its accuracy is verified via the time marching method (Newmark-β algorithm) [56]–[59]

B. EXPERIMENTAL TESTS OF DYNAMIC RESPONSE OF VIBRATING FLIP-FLOW SCREEN

In this section, an experimental test of the dynamic response is performed on a vibrating flip-flow screen with a width of 800 mm, a length of 2700 mm, and an inclination angle of 15°. Fig. 8 shows the schematic of the test process and signal processing. In the experiment, the frequency converter was responsible for adjusting the working speed of the flip-flow screen motor, and the sweeping range was set to 0 to 98.6 rad $\cdot$ s^{-1}. Two acceleration sensors (Coinv, type INV9821, capacity = 100 g, sensitivity = 50 mV $\cdot$ g^{-1}, resolution = 0.1% m $\cdot$ s^{-2}, China) were installed at the centroid of the main and floating screen frame to measure the acceleration signal along the screen surface. The real-time acceleration signals were collected and recorded through a data acquisition instrument (Coinv, type INV3018CT, maximum sampling frequency = 102.4 kHz, spectrum amplitude indication error < 1%, frequency indication and resolution error < 0.01%, number of parallel channels = 8, China) and a computer. By integrating the acceleration signal twice, the displacement of the centroid of the main and the floating screen frame along the screen surface can be obtained. Then, the frequency-domain responses of VFFS can be acquired by extracting the amplitude of the displacement at the steady running stage. The basic parameters of the investigated screen are shown in Table 2.

IV. RESULTS AND DISCUSSION

A. ACCURACY AND NOVELTY OF THE PROPOSED MODEL OF VIBRATING FLIP-FLOW SCREEN

In this subsection, the analytical solution of the nonlinear dynamic equation of VFFS is deduced via the equivalent linearization method, the accuracy of which is verified by the time marching method and dynamic characteristic tests of VFFS. Then, comparing the measurement results with the numerical simulations, the proposed coupling dynamic model that considers the effect of FFSP is shown to describe the movements of the main screen frame and the floating screen frame under steady working conditions more accurately than the classical mechanical model.

1) ANALYTICAL SOLUTIONS OF THE NONLINEAR MODEL OF VIBRATING FLIP-FLOW SCREEN

When the relative amplitude of the main and the floating screen frame $|x_2|$ is less than or equal to the slack length e, the governing Equation (9) for the proposed dynamic model of VFFS can be simplified as:

$$\begin{cases} (m_1+m_2+m_3)\,\ddot{x}_1 + c_{1x}\dot{x}_1 + k_{1x}x_1 \\ \quad -\left(m_2+\dfrac{m_3}{2}\right)\ddot{x}_2 = m_0\omega^2 r\sin(\omega t) \\ \left(m_2+\dfrac{m_3}{2}\right)(\ddot{x}_1-\ddot{x}_2) - c_{2x}\dot{x}_2 - k_{2x}x_2 = 0 \end{cases} \tag{11}$$

Then, the solutions of (11) can be written as:

$$\begin{cases} x_1 = A_1\sin(\omega t-\alpha_1) \\ x_2 = A_2\sin(\omega t-\alpha_2) \end{cases} \tag{12}$$

where A_1 and A_2 are the amplitudes of the displacement of the main screen frame and the relative displacement between two screen frames along the x-direction, respectively; and α_1 and α_2 are the phases of the displacement of the main screen frame and the relative displacement between two screen frames along the x-direction, respectively.

Defining $a_1 = (m_2+m_3/2)\,\omega^2 - k_{2x}, b = c_{2x}\omega, d = k_{1x} - (m_1+m_2+m_3)\,\omega^2, f = c_{1x}\omega, g = (m_2+m_3/2)\,\omega^2, F_0 = m_0\omega^2 r$, we then have:

$$\begin{cases} A_1 = \dfrac{F_0\sqrt{a_1^2+b^2}}{\sqrt{(a_1d+bf+g^2)^2+(a_1f-bd)^2}} \\ A_2 = \dfrac{F_0 g}{\sqrt{(a_1d+bf+g^2)^2+(a_1f-bd)^2}} \\ \alpha_1 = \tan^{-1}\dfrac{a_1^2f+b^2f+bg^2}{a_1^2d+a_1g^2+b^2d} \\ \alpha_2 = \tan^{-1}\dfrac{a_1f-bd}{a_1d+bf+g^2} \end{cases} \tag{13}$$

When the amplitude of the relative displacement between two screen frames $|x_2|$ is greater than the slack length e, there is the nonlinear restoring force of FFSP. Based on the equivalent linearization method, the governing Equation (9) for the proposed dynamic model of VFFS can be written as [60]:

$$\begin{cases} (m_1+m_2+m_3)\,\ddot{x}_1 + c_{1x}\dot{x}_1 + k_{1x}x_1 \\ \quad -\left(m_2+\dfrac{m_3}{2}\right)\ddot{x}_2 = m_0\omega^2 r\sin(\omega t) \\ \left(m_2+\dfrac{m_3}{2}\right)(\ddot{x}_1-\ddot{x}_2) - c_{2x}\dot{x}_2 - (k_{2x}+k_e)\,x_2 \\ \quad = 0 \end{cases} \tag{14}$$

Similarly, the solutions of (14) can be expressed as:

$$\begin{cases} x_1 = B_1\,sin\,(\omega t-\beta_1) \quad (1) \\ x_2 = B_2\,sin\,(\omega t-\beta_2) \quad (2) \end{cases} \tag{15}$$

where k_e in (14) is the equivalent stiffness of the nonlinear restoring force $F_k(x_2)$. To achieve a close approximation between the equivalent elastic force $k_e x_2$ and the nonlinear restoring force $F_k(x_2)$, the integral of the square of the product of the difference between these two forces and the displacement should be minimized for one cycle of motion [61]. Thus:

$$\frac{\partial}{\partial k_e}\int_{-B_2}^{B_2}\left[F_k(x_2)-k_e x_2\right]^2 x_2^2\,dx_2 = 0 \tag{16}$$

Substituting (10) and (15-2) into (16) and merging like items, we then have:

$$k_e = k_3\left(1-\frac{5}{4}\frac{e}{B_2}+\frac{1}{4}\frac{e^5}{B_2^5}\right) \tag{17}$$

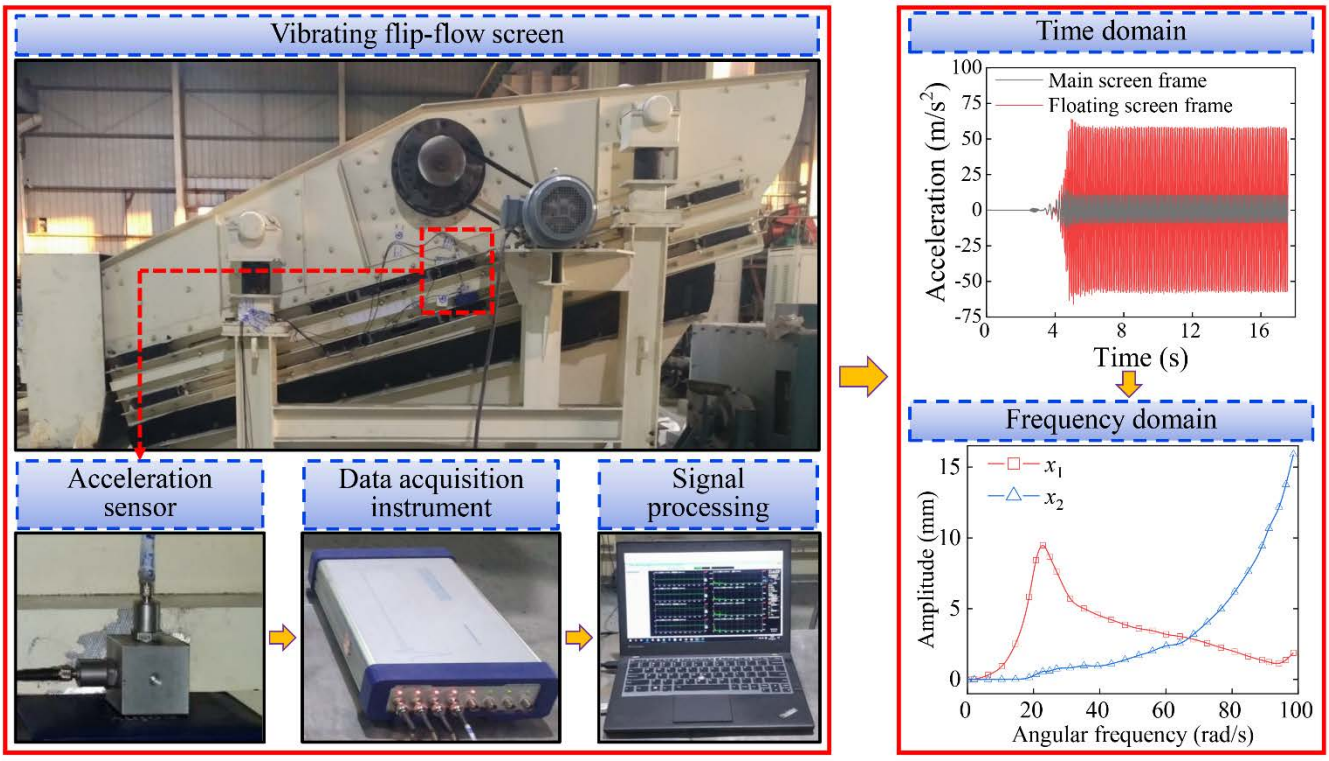

FIGURE 8. Scheme of the experimental tests of vibrating flip-flow screen's dynamic response.

TABLE 2. Parameters for the investigated vibrating flip-flow screen [24].

Symbol	Definition	Unit	Value
m_1	main screen frame mass	kg	916
m_2	floating screen frame mass	kg	310
m_3	shear springs and flip-flow screen panels mass	kg	39
m_0	eccentric blocks mass	kg	48.78
r	eccentricity of the eccentric blocks	m	0.08545
k_{1x}	stiffness of vibration isolation springs	N·m^{-1}	630000
c_{1x}	damping coefficient of vibration isolation springs	N·s·m^{-1}	9866
k_{2x}	stiffness of shear springs	N·m^{-1}	2700000
c_{2x}	damping coefficient of shear springs	N·s·m^{-1}	2605

Defining $a_2 = (m_2 + m_3/2)\,\omega^2 - (k_{2x} + k_e)$, we then have:

$$\begin{cases} B_1 = \dfrac{F_0\sqrt{a_2^2 + b^2}}{\sqrt{\left(a_2 d + bf + g^2\right)^2 + (a_2 f - bd)^2}} & (1) \\ B_2 = \dfrac{F_0 g}{\sqrt{\left(a_2 d + bf + g^2\right)^2 + (a_2 f - bd)^2}} & (2) \\ \beta_1 = \tan^{-1}\dfrac{a_2^2 f + b^2 f + bg^2}{a_2^2 d + a_2 g^2 + b^2 d} & (3) \\ \beta_2 = \tan^{-1}\dfrac{a_2 f - bd}{a_2 d + bf + g^2} & (4) \end{cases} \tag{18}$$

Equation (18-2) is an implicit function of the amplitude of the relative displacement between two screen frames, which is difficult to solve directly and must be simplified.

Defining $A = (m_2 + m_3/2)\,m_0 r$, $C = (m_2 + m_3/2)^2 - (m_1 + m_2 + m_3)\,(m_2 + m_3/2)$, $D = (m_1 + m_2 + m_3)\left(k_{2x} + k_e\right) + (m_2 + m_3/2)\,k_{1x} + c_{1x}c_{2x}$, $E = -k_{1x}\,(k_{2x} + k_e)$, $F = (m_1 + m_2 + m_3)\,c_{2x} + (m_2 + m_3/2)\,c_{1x}$, $G = -\left[c_{1x}\,(k_{2x} + k_e) + c_{2x}k_{1x}\right]$, Equation (18-2) then becomes:

$$\begin{aligned} &\left(B_2^2 C^2 - A^2\right)\omega^8 + B_2^2\left(2CD + F^2\right)\omega^6 \\ &\quad + B_2^2\left(2CE + D^2 + 2FG\right)\omega^4 + B_2^2\left(2DE + G^2\right)\omega^2 \\ &= -B_2^2 E^2 \end{aligned} \tag{19}$$

As shown in (19), this is an eighth-order polynomial in ω. Eight solutions are possible, but only the positive real-valued solutions for ω are physically meaningful. For the results shown before, the frequency ω is given, and the amplitudes

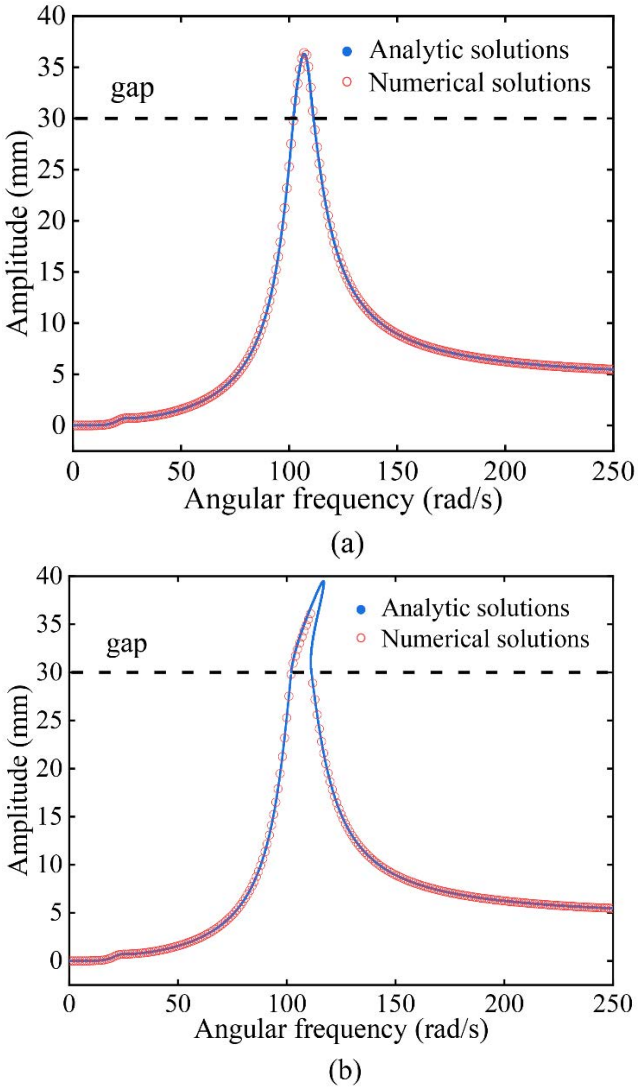

FIGURE 9. Comparison of the analytic and numerical solutions of the proposed nonlinear dynamics model of vibrating flip-flow screen: (a) Weak nonlinearity, (b) Strong nonlinearity.

are computed from the amplitude-frequency relationship. Conversely, another efficient alternative to solve (19) is to prescribe the amplitude B_2 and solve the equation for ω. Then, substituting B_2 and ω into (18-1), (18-3), and (18-4), we can obtain B_1, β_1, and β_2, respectively.

2) DIFFERENCES BETWEEN ANALYTICAL SOLUTIONS AND TIME MARCHING RESULTS OF VIBRATING FLIP-FLOW SCREEN'S NONLINEAR EQUATIONS

As shown in Fig. 9, the accuracy of the analytical solution is validated using the proposed nonlinear dynamics model as a prototypical system compared to the time marching solution in cases of weak nonlinearity ($e = 30$ mm, $k_3 = 5 \times 10^5$ N $\cdot$ m^{-1}) and strong nonlinearity ($e = 30$ mm, $k_3 = 5 \times 10^6$ N$\cdot$m^{-1}). Other dynamic parameters are shown in Table 2.

These results indicate that when the nonlinearity is weak, the results for the two different methods shown to be approximately identical. In the strong nonlinear case, the steady-state solution of the relative amplitude of those two frames obtained by the equivalent linear method also matches the time marching solution well except for the excitation frequencies near the second-order resonance region. This is due to although numerical integration could give stable solutions, whether periodic or not, it is difficult to track the multi-value regimes [62], [63] In addition, when the relative amplitude between two screen frames exceeds the FFSP slack length, the resonant peak value shifts toward a higher frequency region, demonstrating the hardening nonlinearity of the system caused by the tensile deformation of FFSP. The system also exhibits multi-value features around the resonance region. Due to the transition between the noncontact state and the contact state, discontinuities of the slope of the resonance curve occur at the transition points [62], [64].

This subsection verifies the accuracy of the equivalent linear method for solving the proposed coupling mechanical model of VFFS; therefore, this method is used in the calculations below.

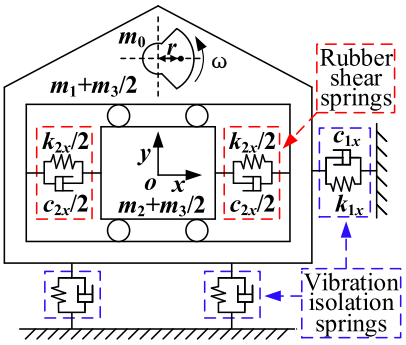

FIGURE 10. Classical mechanical model of vibrating flip-flow screen.

3) COMPARISON OF DYNAMICS BETWEEN EXPERIMENTS AND DIFFERENT MECHANICAL MODELS OF VIBRATING FLIP-FLOW SCREEN

To verify the accuracy of the constructed coupling mechanical model of VFFS considering the tensile stress of FFSP, the dynamic responses of the classical model and the proposed mechanical model of VFFS are compared with experimental results.

The classical mechanical model to describe the dynamic response of VFFS is shown in Fig. 10, the parameters of which are the same as those in Fig. 7. This model's governing equation is:

$$\begin{cases} (m_1 + m_2 + m_3)\,\ddot{x}_1 + c_{1x}\dot{x}_1 + k_{1x}x_1 \\ \quad - \left(m_2 + \dfrac{m_3}{2}\right)\ddot{x}_2 = m_0\omega^2 r\sin(\omega t) \\ \left(m_2 + \dfrac{m_3}{2}\right)(\ddot{x}_1 - \ddot{x}_2) - c_{2x}\dot{x}_2 - k_{2x}x_2 = 0 \end{cases} \tag{20}$$

Similarly, its solutions are (12).

Based on the finite element analysis of FFSP in Section 2, the stiffness of FFSP is 121000 N $\cdot$ m^{-1}. The investigated vibrating flip-flow screen contains 8 screen panels, the

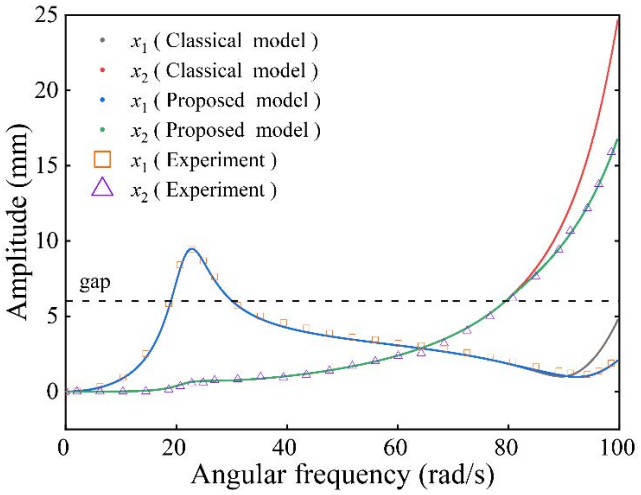

FIGURE 11. Comparison of the amplitude-frequency curves of different dynamic models and the experimental results of vibrating flip-flow screen.

slack length of which is $e = 6$ mm. However, when the screen is running, the adjacent screen panels generate tensile stress alternatively because they move in opposite directions. Therefore, the global stiffness of FFSP $k_3 = 484000\ \mathrm{N \cdot m^{-1}}$. Fig. 11 shows the amplitude-frequency responses when using the experimental tests, in addition to the results obtained via the classical model and the proposed VFFS model. Other dynamic parameters are shown in Table 2. This result indicates that when the relative amplitude is less than the slack length, the results for these two models agree and are approximately identical to the experimental measurements. However, when the relative amplitude is beyond the slack length, the discrepancy of the amplitudes between the classical model and the experimental tests gradually becomes significant with increasing angular frequency. The proposed model matches well with the measurement results, as before; thus, the proposed coupling mechanical model considering the effect of FFSP can better describe the dynamic response of VFFS compared with the classical model.

In addition, error analysis of the relative amplitude between two screen frames is performed, as shown in Fig. 12. The largest error of the novel coupling mechanics model is 5.23% at an angular frequency of 80.8 rad $\cdot$ s^{-1} for the case of $x_2 > e$. This result occurs because the relative amplitude is 6.44 mm, which is marginally higher than the FFSP slack length (6 mm), when the angular frequency is 80.8 rad $\cdot$ s^{-1}. Also, the higher-order harmonic components of the screen panels may affect the dynamics of the main and floating screen frames.

However, the error of the classical model increases with increasing angular frequency, and its minimum and largest errors are 5.56% and 40.69%, respectively. This result occurs because the classical model does not consider the effect of FFSP. The greater the angular frequency is, the greater the relative amplitude of those two frames is. Starting from 80.8 rad$\cdot$s^{-1}, the force generated from the tensile deformation

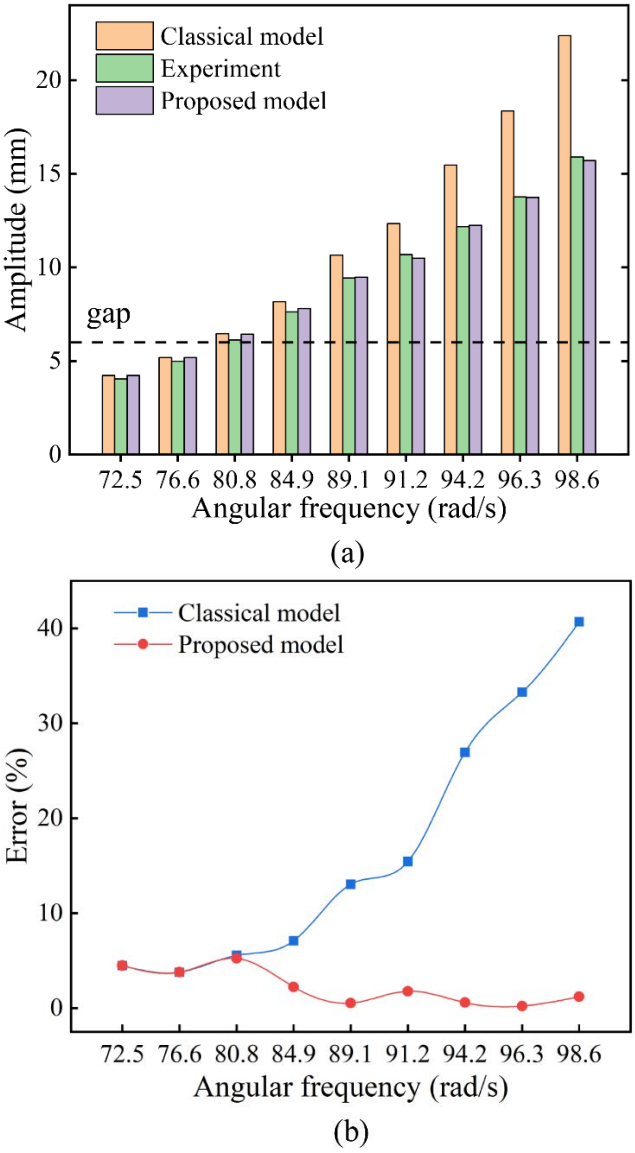

FIGURE 12. Error analysis of the relative amplitude of the proposed and classical mechanical models of vibrating flip-flow screen: (a) Amplitude, (b) Error.

of FFSP strongly affects the motions of the main and floating screen frames. Therefore, the capability and reasonability of the proposed mechanical model of VFFS have been verified.

B. EFFECTS OF FLIP-FLOW SCREEN PANEL ON DYNAMICS OF VIBRATING FLIP-FLOW SCREEN

1) EFFECTS OF THE STIFFNESS OF FLIP-FLOW SCREEN PANELS ON THE DYNAMIC RESPONSE OF VIBRATING FLIP-FLOW SCREEN

The FFSP slack length is 6 mm, the corresponding stiffness is 0%, 25%, 50%, 100%, and 200% of the shear springs stiffness, and other simulation parameters are shown in Table 2. The effect of flip-flow screen panel stiffness on the dynamic response of VFFS is shown in Fig. 13.

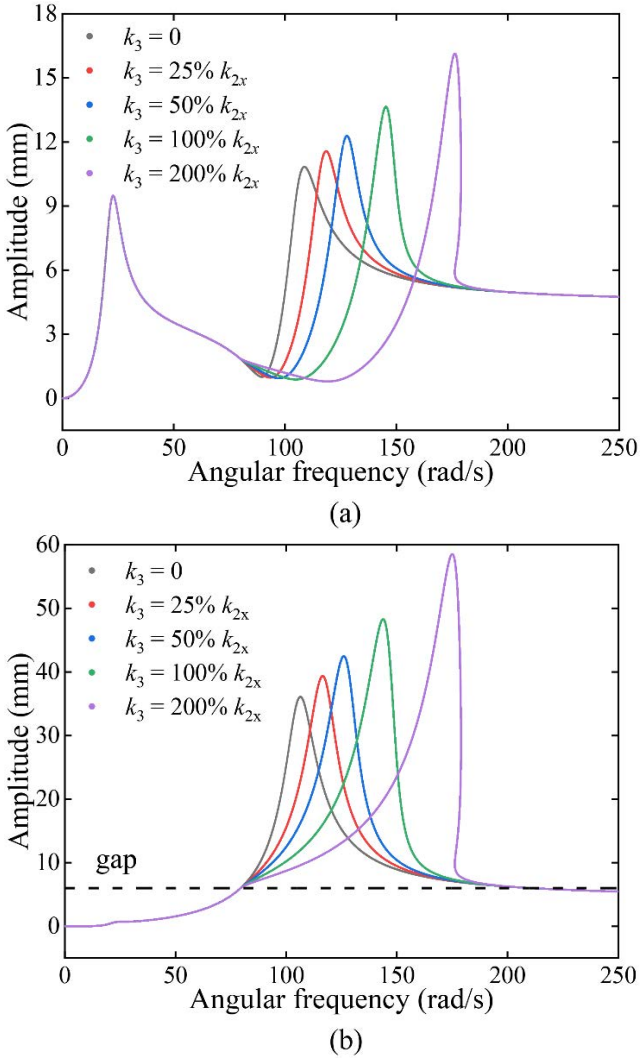

FIGURE 13. Effect of the stiffness of flip-flow screen panels on the dynamic response of vibrating flip-flow screen: (a) Displacement amplitude of the main screen frame, (b) Relative amplitude of the main and the floating screen frame.

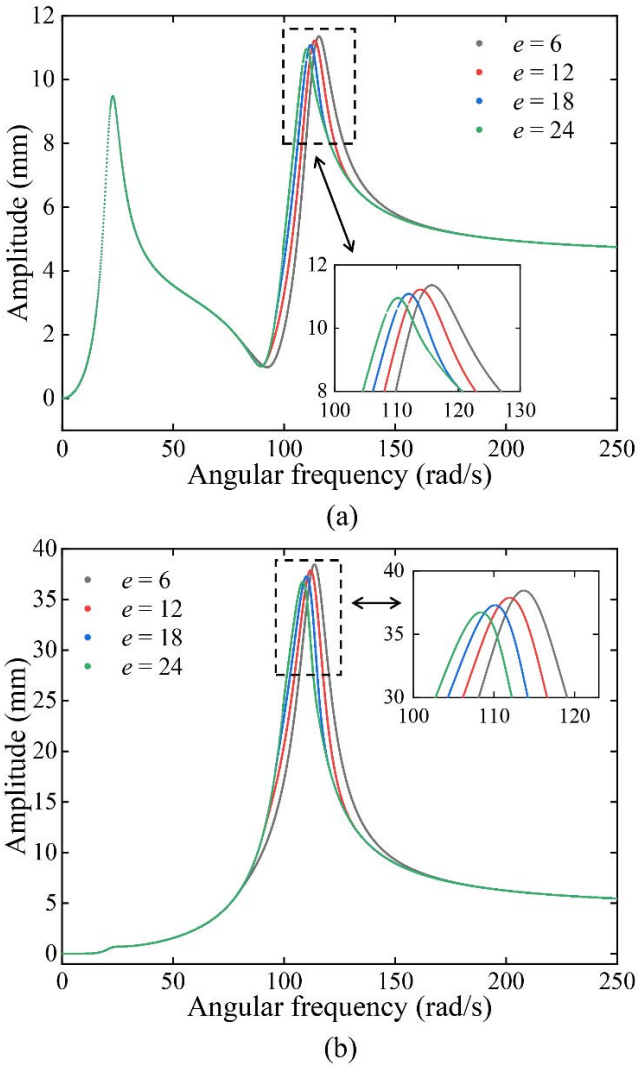

FIGURE 14. Effect of the slack length of flip-flow screen panels on the dynamic response of vibrating flip-flow screen: (a) Displacement amplitude of the main screen frame, (b) Relative amplitude of the main and the floating screen frame.

When the stiffness of FFSP is 0, it is equivalent to the dynamic response of the classical linear mechanical model ignoring the effect of FFSP. When the relative amplitude is beyond the slack length, the stiffness of FFSP has a marked impact on the amplitude-frequency curve of the main and floating screen frames. Also, the classical linear model is no longer suitable for describing the dynamic response of VFFS.

Based on the proposed coupled mechanical model of VFFS considering the effect of FFSP, the second-order natural frequencies of the screen body shift rightward with increasing FFSP stiffness, and the corresponding resonance peaks increase. The curve of the relative amplitude of the main and the floating screen frame near the slack length on the left side of the second-order resonance zone is more stable, which is conducive to VFFS loading stability [15].

2) EFFECTS OF THE SLACK LENGTH OF FLIP-FLOW SCREEN PANELS ON THE DYNAMIC RESPONSE OF VIBRATING FLIP-FLOW SCREEN

The global stiffness of FFSP is $k_3 = 484000\ \mathrm{N \cdot m^{-1}}$; the slack lengths are considered to be 6, 12, 18, and 24 mm; and the other dynamic parameters remain constant. The influence of the slack length of flip-flow screen panels on the dynamic response of VFFS is shown in Fig. 14. When the slack lengths are 6, 12, 18, and 24 mm, the second-order natural frequencies of the screen body are 115.7, 113.9, 112.0, and 110.2 rad $\cdot$ $\mathrm{s^{-1}}$, respectively the displacement amplitudes of the main screen frame are 11.36, 11.22, 11.09, and 10.96 mm, the relative amplitudes of the main and the floating screen frame are 38.45, 37.87, 37.29, and 36.73 mm. As the slack length increases, the second-order natural frequency of the screen body gradually shifts leftward, and the amplitude of the second-order resonance region decreases correspondingly.

V. CONCLUSION

This study numerically investigates the dynamic characteristics of FFSP and then proposes an experimentally validated mechanical model of VFFS. Using this model, the nonlinear effect of FFSP on the dynamic response of VFFS is explored in detail. Based on the results of this study, the following conclusions can be drawn:

1) When the tension value is greater than or equal to two times the relative amplitude, the screen panel experiences tensile stress throughout its movement, and the dominant source of the force is tensile deformation. The PSD of the force signal only has a peak at the frequency of excitation. When the tension value is less than two times the relative amplitude and greater than zero, there is both tension and slack during the screen panel's movement, and the screen panel's force is due to the flexural stress, which is caused by the inertial force, and the tensile stress, which is caused by the tensile deformation. The force consists of a component corresponding to the fundamental frequency and of higher-order harmonic components, which are the second and third harmonics, respectively. The peak PSD corresponding to the fundamental frequency is the highest, followed by the second and third harmonics. When the tension value is less than or equal to zero, the screen panel is always slack during its precession, the force of the screen panel is only the flexural stress generated from the inertial force, which fluctuates around zero, and its PSD is nearly zero.
2) Because the relative amplitude is less than the slack length, the results produced by the proposed and classical models completely coincide and are approximately identical to the experimental measurements. However, when the relative amplitude exceeds the slack length, the discrepancy of the amplitudes between the classical model and the experimental tests gradually becomes larger with increasing angular frequency, and the proposed model agrees with the experimental measurements. Therefore, the working state of VFFS can be described more accurately by the proposed novel model than the classical dynamic model.
3) With increasing screen-panel stiffness, the second-order natural frequencies of the screen body shift rightward, and the corresponding resonance peaks increase. Conversely, as the slack length increases, the second-order natural frequency of the screen body gradually shifts leftward, and the amplitude of the second-order resonance region decreases correspondingly.

REFERENCES

[1] H. Akbari, L. A. Ackah, and M. K. Mohanty, "Development of a new fine particle dry separator," *Minerals Metall. Process.*, vol. 35, no. 2, pp. 77–86, May 2018.

[2] H. Dong, C. Liu, Y. Zhao, and L. Zhao, "Review of the development of dry coal preparation theory and equipment," in *Proc. 1st Int. Workshop Hydraulic Equip. Support Syst. Mining*, Huludao, China, 2012, pp. 239–243.

[3] H. Akbari, L. Ackah, and M. Mohanty, "Performance optimization of a new air table and flip-flow screen for fine particle dry separation," *Int. J. Coal Preparation Utilization*, vol. 40, no. 9, pp. 581–603, Sep. 2020.

[4] G. W. Delaney, P. W. Cleary, M. Hilden, and R. D. Morrison, "Testing the validity of the spherical DEM model in simulating real granular screening processes," *Chem. Eng. Sci.*, vol. 68, no. 1, pp. 215–226, Jan. 2012.

[5] P. Aqueveque, L. Radrigan, A. S. Morales, and E. Willenbrinck, "Development of a cyber-physical system to monitor early failures detection in vibrating screens," *IEEE Access*, vol. 9, pp. 145866–145885, 2021.

[6] A. Davoodi, M. Bengtsson, E. Hulthén, and C. Evertsson, "Effects of screen decks' aperture shapes and materials on screening efficiency," *Minerals Eng.*, vol. 139, pp. 1–9, Aug. 2019.

[7] H. Jiang, W. Wang, Z. Zhou, H. Jun, P. Wen, Y. Zhao, C. Duan, L. Zhao, Z. Luo, and C. Liu, "Simultaneous multiple parameter optimization of variable-amplitude equal-thickness elastic screening of moist coal," *Powder Technol.*, vol. 346, pp. 217–227, Mar. 2019.

[8] L. Li and X. Chen, "Multi-frequency vibration synchronization and stability of the nonlinear screening system," *IEEE Access*, vol. 7, pp. 171032–171045, 2019.

[9] Z. Gangfeng, Z. Jinbo, X. Wandong, and L. Shili, "Banana flip-flow screen benefits coal preparation," *Filtration Separat.*, vol. 53, no. 4, pp. 38–41, Jul. 2016.

[10] G. Zhao, X. Wang, C. Yu, S. Liu, J. Zhou, and G. Zhu, "Research on static and dynamic characteristics of shear spring of the vibrating flip-flow screen," *Symmetry*, vol. 12, no. 10, pp. 1–25, Oct. 2020.

[11] Q. Guo and G. Gong, "Application of flip flow screen in Sihe coal preparation plant," in *XVIII International Coal Preparation Congress*. Cham, Switzerland: Springer, 2016, pp. 913–918.

[12] L. Peng, F. Li, H. Dong, C. Liu, Y. Zhao, and C. Duan, "Characteristics analysis of a novel centralized-driving flip-flow screen," *Int. J. Mining Sci. Technol.*, vol. 24, no. 2, pp. 195–200, Mar. 2014.

[13] O. A. Makinde, B. I. Ramatsetse, and K. Mpofu, "Review of vibrating screen development trends: Linking the past and the future in mining machinery industries," *Int. J. Mineral Process.*, vol. 145, pp. 17–22, Dec. 2015.

[14] B. Zhang, G. Zhu, B. Lv, and G. Yan, "A novel and effective method for coal slime reduction of thermal coal processing," *J. Cleaner Prod.*, vol. 198, pp. 19–23, Oct. 2018.

[15] A. Noble and G. H. Luttrell, "A review of state-of-the-art processing operations in coal preparation," *Int. J. Mining Sci. Technol.*, vol. 25, no. 4, pp. 511–521, Jul. 2015.

[16] L. Peng, H. Jiang, X. Chen, D. Liu, H. Feng, L. Zhang, Y. Zhao, and C. Liu, "A review on the advanced design techniques and methods of vibrating screen for coal preparation," *Powder Technol.*, vol. 347, pp. 136–147, Apr. 2019.

[17] C. Yu, X. Wang, S. Gong, K. Pang, G. Zhao, Q. Zhou, D. Lin, and N. Xu, "Stability analysis of the screening process of a vibrating flip-flow screen," *Minerals Eng.*, vol. 163, pp. 1–13, Mar. 2021.

[18] S. Gong, S. Oberst, and X. Wang, "An experimentally validated rubber shear spring model for vibrating flip-flow screens," *Mech. Syst. Signal Process.*, vol. 139, pp. 1–15, May 2020.

[19] X. Xiong, L. Niu, C. Gu, and Y. Wang, "Vibration characteristics of an inclined flip-flow screen panel in banana flip-flow screens," *J. Sound Vib.*, vol. 411, pp. 108–128, Dec. 2017.

[20] J. Tang, L. Niu, X. Xiong, and S. Jie, "Viscoelasticity of rubber springs affects vibration characteristics of a flip-flow screen with the high G value," *IEEE Access*, vol. 8, pp. 26950–26965, 2020.

[21] G. Zhao, X. Wang, D. Lin, N. Xu, C. Yu, and R. Geng, "Study of double-deck vibrating flip-flow screen based on dynamic stiffness characteristics of shear springs," *Minerals*, vol. 11, no. 9, pp. 1–17, Sep. 2021.

[22] S. Gong, X. Wang, and S. Oberst, "Non-linear analysis of vibrating flip-flow screens," in *Proc. 3rd Int. Conf. Design Manuf. Eng.*, Melbourne, VIC, Australia, 2018, pp. 1–4.

[23] J. Wu, C. Liu, H. Jiang, and B. Zhang, "A vibration-test-based calculation method of screening material mass of a mining crank-link type flip-flow screen," *Energy Source A, Recovery, Utilization, Environ. Effects*, pp. 1–21, Jun. 2020, doi: 10.1080/15567036.2020.1778139.

[24] C. Yu, X. Wang, K. Pang, G. Zhao, and W. Sun, "Dynamic characteristics of a vibrating flip-flow screen and analysis for screening 3 mm iron ore," *Shock Vib.*, vol. 2020, pp. 1–12, May 2020.

[25] E. Zhou, G. Yan, X. Weng, Z. Zhang, P. Zhao, and B. Zhang, "A novel and low cost coal separation process: Combination of deep screening classification and gravity separation," *Powder Technol.*, vol. 367, pp. 568–575, May 2020.

[26] R. Talebitooti, H. D. Gohari, and M. R. Zarastvand, "Multi objective optimization of sound transmission across laminated composite cylindrical shell lined with porous core investigating non-dominated sorting genetic algorithm," *Aerosp. Sci. Technol.*, vol. 69, pp. 269–280, Oct. 2017.
[27] R. Talebitooti, M. Zarastvand, and H. Darvishgohari, "Multi-objective optimization approach on diffuse sound transmission through poroelastic composite sandwich structure," *J. Sandwich Struct. Mater.*, vol. 23, no. 4, pp. 1221–1252, Jun. 2019.
[28] Y. Zhao, C. Liu, M. Fan, and L. Wei, "Research on acceleration of elastic flip–flow screen surface," *Int. J. Mineral Process.*, vol. 59, no. 4, pp. 267–274, Jul. 2000.
[29] H. Zhai and X. Ning, "Acceleration recommendation model of the flip-flow screen based on basic dynamics of the screen surface," (in Chinese), *Mining Process. Equip.*, vol. 33, no. 4, pp. 41–43, 2005.
[30] M. R. Zarastvand, M. Ghassabi, and R. Talebitooti, "A review approach for sound propagation prediction of plate constructions," *Arch. Comput. Methods Eng.*, vol. 28, no. 4, pp. 2817–2843, Jun. 2021.
[31] B. Chen, C. Yu, S. Gong, and X. Wang, "Dynamic characteristics of LIWELL flip-flow screen panel and particle movement," *Chem. Eng. Sci.*, vol. 245, pp. 1–11, Dec. 2021.
[32] C. Yu, R. Geng, and X. Wang, "A numerical study of separation performance of vibrating flip-flow screens for cohesive particles," *Minerals*, vol. 11, no. 6, pp. 1–14, Jun. 2021.
[33] B. Wu, X. Zhang, L. Niu, X. Xiong, Z. Dong, and J. Tang, "Research on sieving performance of flip-flow screen using two-way particles-screen panels coupling strategy," *IEEE Access*, vol. 7, pp. 124461–124473, 2019.
[34] L. Liu, S. Lu, T. Zhao, and Z. Wang, "Spectrum truncation power iteration for agnostic matrix phase retrieval," *IEEE Trans. Signal Process.*, vol. 69, pp. 3991–4006, 2021.
[35] Y. Lim, T. Saramaki, P. S. R. Diniz, and Q. Liu, "Fast convergence method for scaling window sidelobe magnitude," *IEEE Signal Process. Lett.*, vol. 28, pp. 2078–2081, 2021.
[36] C. Moreau, T. Devogele, C. de Runz, V. Peralta, E. Moreau, and L. Etienne, "A fuzzy generalisation of the Hamming distance for temporal sequences," in *Proc. IEEE Int. Conf. Fuzzy Syst. (FUZZ-IEEE)*, Jul. 2021, pp. 1–8.
[37] J. Baumgart, C. Fritzsche, and S. Marburg, "Infrasound of a wind turbine reanalyzed as power spectrum and power spectral density," *J. Sound Vib.*, vol. 7, pp. 1–5, Jun. 2021.
[38] M. Aslam, I. U. Haq, M. S. Rehan, F. Ali, A. Basit, M. I. Khan, and M. N. Arbab, "Health analysis of transformer winding insulation through thermal monitoring and fast Fourier transform (FFT) power spectrum," *IEEE Access*, vol. 9, pp. 114207–114217, 2021.
[39] W. Liu, S. Zheng, Z. Deng, K. Wang, W. Lin, J. Lei, Y. Jin, and H. Liu, "Multi-scene Doppler power spectrum modeling of LEO satellite channel based on atlas fingerprint method," *IEEE Access*, vol. 9, pp. 11811–11822, 2021.
[40] Y. Huang, B. Dian, and W. Chappell, "Spectral signature decay analysis and new tapered coaxial transmission line spectrometer design," in *IEEE MTT-S Int. Microw. Symp. Dig.*, Seattle, WA, USA, Jun. 2013, pp. 4630–4635.
[41] N. Rubert and T. Varghese, "Coherence of ultrasound radiofrequency echoes from the liver estimated using multi-taper calculation," in *Proc. IEEE 10th Int. Symp. Biomed. Imag., From Nano Macro*, San Francisco, CA, USA, Apr. 2013, pp. 724–727.
[42] R. Talebitooti, M. R. Zarastvand, and H. D. Gohari, "The influence of boundaries on sound insulation of the multilayered aerospace poroelastic composite structure," *Aerosp. Sci. Technol.*, vol. 80, pp. 452–471, Sep. 2018.
[43] L. Quan, J. Gao, C. Guo, S. Wu, and J. Yao, "Dynamic model and response analysis of bionic hydraulic pipeline based on vascular physiological structure," *IEEE Access*, vol. 7, pp. 67564–67575, 2019.
[44] Y. D'Mello, J. Skoric, L. Moukarzel, S. Hakim, and D. V. Plant, "Wearable fiber optic sensors for biomechanical sensing via joint angle detection," in *Proc. 41st Annu. Int. Conf. IEEE Eng. Med. Biol. Soc. (EMBC)*, Berlin, Germany, Jul. 2019, pp. 3221–3225.
[45] N. C. Rouze, A. Caenen, and K. R. Nightingale, "Wave speeds and Green's tensors for shear wave propagation in incompressible, hyperelastic materials with uniaxial stretch," in *Proc. IEEE Int. Ultrason. Symp. (IUS)*, Glasgow, U.K., Oct. 2019, pp. 427–430.
[46] J. Yan, C. Liu, S. Zhang, and H. Zhou, "Dynamic analysis of sieving plate of centralized-driven flip-flow screens," (in Chinese), *Mining Mach.*, vol. 39, no. 4, pp. 95–97, Jan. 2011.
[47] M. Zarastvand, M. Asadijafari, and R. Talebitooti, "Improvement of the low-frequency sound insulation of the poroelastic aerospace constructions considering Pasternak elastic foundation," *Aerosp. Sci. Technol.*, vol. 112, pp. 1–20, May 2021.
[48] H. D. Gohari, M. Zarastvand, and R. Talebitooti, "Acoustic performance prediction of a multilayered finite cylinder equipped with porous foam media," *J. Vib. Control*, vol. 26, nos. 11–12, pp. 899–912, Jan. 2020.
[49] S. Qiu, H. Ren, H. Li, Y. Zhou, and D. Wang, "Multibody dynamics model and simulation for the totally enclosed lifeboat lowered from ship in rough seas," *IEEE Access*, vol. 9, pp. 32171–32187, 2021.
[50] S. S. Rao, "Two-degree-of-freedom systems," in *Mechanical Vibrations*, 5th ed. Albuquerque, NM, USA: Pearson, 2010, ch. 5, sec. 6, pp. 494–497.
[51] J. Lin, Y. Zhao, Q. Zhu, S. Han, H. Ma, and Q. Han, "Nonlinear characteristic of clamp loosing in aero-engine pipeline system," *IEEE Access*, vol. 9, pp. 64076–64084, 2021.
[52] Y. S. Hamed and H. K. Alkhathami, "On the nonlinear vibrations and stability analysis of a plate-cavity system with a nonlinear restoring force," *IEEE Access*, vol. 9, pp. 20423–20439, 2021.
[53] Q. Zhang and Z. Liu, "A novel piecewise affine model for vehicle lateral dynamics," *IEEE Access*, vol. 6, pp. 78493–78502, 2018.
[54] R. Iervolino, S. Trenn, and F. Vasca, "Asymptotic stability of piecewise affine systems with Filippov solutions via discontinuous piecewise Lyapunov functions," *IEEE Trans. Autom. Control*, vol. 66, no. 4, pp. 1513–1528, Apr. 2021.
[55] S. Scalzi, P. Tomei, and C. M. Verrelli, "Nonlinear control techniques for the heart rate regulation in treadmill exercises," *IEEE Trans. Biomed. Eng.*, vol. 59, no. 3, pp. 599–603, Mar. 2012.
[56] L. Liu, J. P. Thomas, E. H. Dowell, P. Attar, and K. C. Hall, "A comparison of classical and high dimensional harmonic balance approaches for a Duffing oscillator," *J. Comput. Phys.*, vol. 215, no. 1, pp. 298–320, Jun. 2006.
[57] N. M. Newmark, "A method of computation for structural dynamics," *J. Eng. Mech. Division*, vol. 85, no. 3, pp. 67–94, 1959.
[58] Y. Zhao, Y. Liu, X. Xin, S. Yu, H. Ma, and Q. Han, "Dynamic modelling considering nonlinear factors of coupled spur gear system and its experimental research," *IEEE Access*, vol. 8, pp. 84971–84980, 2020.
[59] S. Wang, A. Xieeryazidan, X. Zhang, and J. Zhou, "An improved computational method for vibration response and radiation noise analysis of two-stage gearbox," *IEEE Access*, vol. 8, pp. 85973–85988, 2020.
[60] Z. Zhang, S. Cao, and C. Ruan, "Statistical linearization analysis of a hydropneumatic suspension system with nonlinearity," *IEEE Access*, vol. 6, pp. 73760–73773, 2018.
[61] B. Wen, Y. Li, P. Xu, and Q. Han, "Equivalent linear method and harmonic balance method," in *Nonlinear Vibration in Engineering*, 1st ed. Beijing, China: Science Press, 2007, ch. 2, sec. 1, pp. 32–37.
[62] Z. Zhang, X. Ma, H. Hua, and X. Liang, "Nonlinear stochastic dynamics of a rub-impact rotor system with probabilistic uncertainties," *Nonlinear Dyn.*, vol. 102, no. 4, pp. 2229–2246, Nov. 2020.
[63] W. Sun, Z. Jiang, X. Xu, Q. Han, and F. Chu, "Harmonic balance analysis of output characteristics of free-standing mode triboelectric nanogenerators," *Int. J. Mech. Sci.*, vol. 207, Oct. 2021, Art. no. 106668.
[64] G. V. Groll and D. J. Ewins, "The Harmonic balance method with arc-length continuation in rotor/stator contact problems," *J. Sound Vib.*, vol. 241, no. 2, pp. 223–233, Mar. 2001.

DONGDONG LIN was born in Weinan, Shaanxi, China, in 1991. He received the B.E. degree from the School of Chemical and Environmental Engineering, China University of Mining and Technology, Beijing (CUMTB), in 2016, where he is currently pursuing the Ph.D. degree.

His research interests include nonlinear dynamics and mechanical engineering.

NINGNING XU was born in Liaoyang, Liaoning, China, in 1995. He is currently pursuing the Ph.D. degree with the School of Chemical and Environmental Engineering, China University of Mining and Technology, Beijing.

His research interests include dynamics analysis and simulation of flip-flow screens.

CHI YU was born in Shenyang, Liaoning, China, in 1994. He received the B.E. degree from the School of Chemical and Environmental Engineering, China University of Mining and Technology, Beijing (CUMTB), in 2016, where he is currently pursuing the Ph.D. degree.

His research interests include dynamics and screening of fine materials.

RUNHUI GENG was born in Handan, Hebei, China, in 1998. He is currently pursuing the Ph.D. degree with the School of Chemical and Environmental Engineering, China University of Mining and Technology, Beijing.

His research interests include mechanical dynamics modeling and screening machine.

XINWEN WANG received the Ph.D. degree from the China University of Mining and Technology, Xuzhou, in 2001.

He is currently a Professor with the China University of Mining and Technology, Beijing. He has published over 60 journal articles. His research interests include solid particle transportation, screening and dehydration equipment, and mechanical vibration.

SANPENG GONG received the Ph.D. degree from the China University of Mining and Technology, Beijing, in 2020.

He is currently a Lecturer of mechanical engineering with Henan Polytechnic University. He has published over ten journals and conference papers. His research interests include mining equipment, vibration, and nonlinear dynamics.